

Extreme Multi-Directional Waves

T.B. Johannessen¹ & C. Swan²

Abstract

The present paper concerns the nonlinear description of large waves in which the wave energy is spread in both the frequency and the directional domains. A new series of experimental observations are briefly described in which a large number of deep-water focused wave groups were generated in a large wave basin. For each combination of frequency bandwidth and directional spread the intensity of the wave, measured in terms of a linear amplitude sum, was varied from a near-linear condition to the limit of incipient wave breaking. Comparisons between this laboratory data and a new fully nonlinear, multi-directional, numerical model are used to validate the modelling procedure and highlight the importance of the directionality. In particular, the results show that for a given linear amplitude sum an increase in the directional spread leads to a reduction in the magnitude of the nonlinear wave-wave interactions. Conversely, the maximum nonlinear crest elevation, observed just prior to the onset of wave breaking, increases with the directional spread assuming the frequency bandwidth remains constant. From a practical perspective, the paper demonstrates that an accurate representation of an extreme ocean wave requires a model that incorporates nonlinearity, unsteadiness and directionality. The present model satisfies these requirements.

1. Introduction

It is well known that the largest ocean waves, which are by definition highly nonlinear, do not arise as part of a regular wave train, but occur as individual events within a random or irregular sea. Indeed, field data confirms that the most severe storms are typically characterised by a relatively broad-banded frequency spectrum implying a

¹ Senior Engineer, Kvaerner Oil and Gas, Oslo, Norway

² Reader, Department of Civil and Environmental Engineering, Imperial College, London, SW7 2BU.

wide distribution of energy within the frequency domain. As a result, the largest waves, arising due to the constructive interference or focusing of the frequency components (see Tromans et al., 1991), only arise at one point in space and time and are thus commonly referred to as transient waves. More recently, it has also been shown that such waves will have a significant distribution of energy in the directional domain. For example, Jonathan et al. (1994) have considered several severe storms arising in the northern North Sea, and show that the wind waves have a typical directional spread corresponding to a normal distribution with a standard deviation of 30° .

Having established that large wave events are nonlinear, transient and directional, it is perhaps surprising to note that the commonly applied design solutions either include the nonlinearity or the unsteadiness, but seldom both, and typically neglect the underlying directionality. For example, a linear random wave theory provides a first approximation to the dispersive properties of a sea state, and hence models the transient nature of individual waves, but entirely neglects the nonlinearity. In contrast, a nonlinear regular (or steady) wave theory, either based upon a Stokes' expansion (Fenton, 1985) or a stream function formulation (Dean, 1965), includes the nonlinearity but neglects the unsteadiness. More recently, an alternative design solution proposed by Baldock and Swan (1994) includes both the nonlinearity and the unsteadiness, and has been shown to be effective in a wide range of water depths (Smith and Swan, 1996). However, even in this latter model the omission of directionality represents a serious restriction.

Evidence as to the importance of directionality in the evolution of large waves has recently come to light in comparisons between two-dimensional laboratory data and field measurements. For example, Baldock et al. (1996) provides observations of extreme two-dimensional wave groups, produced by the focusing of energy due to frequency dispersion. These results show that the nonlinear wave-wave interactions may increase the maximum crest elevation by as much as 30% above that predicted by the linear sum of the underlying wave components. In contrast, the analysis of field data (Rozario et al., 1993) suggests that while nonlinearity is undoubtedly important, the corresponding increase in the maximum crest elevation is substantially less than 30%. An obvious explanation for this difference lies in the directionality of the field data.

The present paper will address this point and will provide comparisons between a fully nonlinear, multi-directional, wave model and a new series of laboratory observations undertaken in a large wave basin. Section 2 commences with a brief description of the numerical model; while section 3 outlines the nature of the experimental study. Comparisons between these results are provided in section 4, with particular attention given to both the maximum crest elevations and the underlying water particle kinematics. In section 5 some additional numerical calculations are provided to examine the nature of the nonlinear wave-wave interactions arising in the vicinity of the largest wave crests, and in particular their dependence upon the directionality of the wave field. The paper concludes in section 6 by highlighting the practical implications of the present study.

2. Numerical Modelling

The numerical model outlined within this section is an extension of the two-dimensional time-stepping formulation originally proposed by Fenton and Rienecker (1980). In its original form this scheme represents one of several potential flow solutions, each capable of accurately modelling the evolution of a two-dimensional nonlinear wave train (e.g. Longuet-Higgins and Cokelet, 1976, Dold and Peregrine, 1984, and Dommermuth et al., 1988). In the context of the present study the scheme outlined by Fenton and Rienecker (1980) was adopted because, although it is less efficient (computationally) than many of the other schemes, it is expandable to three-dimensions. Assuming that a fluid flow is both inviscid and irrotational a velocity potential, ϕ , defined by $\underline{u}=\nabla\phi$, where \underline{u} is the velocity vector, can be expressed as:

$$\Phi(x,y,z,t) = \sum_{m=0}^{\infty} \text{Cos}(mk_y y) \sum_{n=0}^{\infty} \left(A_{nm} \text{Cos}(nk_x x) + B_{nm} \text{Sin}(nk_x x) \right) \frac{\cosh(k_{nm}[z+d])}{\sinh(k_{nm}d)} \quad (1)$$

where (x,y,z) are the usual Cartesian co-ordinates with z defined vertically upwards from the mean water level, $z=-d$ defines the bottom boundary, and (x,y) are the horizontal co-ordinates which are orientated such that the x -axis defines the mean wave direction (see section 3 below). Furthermore, $k_{nm} = \sqrt{(nk_x^2 + mk_y^2)}$ where (k_x, k_y) define the large fundamental length scales, $\lambda_x=2\pi/k_x$ and $\lambda_y=2\pi/k_y$, over which the solution is assumed periodic in the x and y directions respectively. Likewise, the free surface elevation, which must be similarly periodic in space, is given by:

$$\eta(x,y,t) = \sum_{m=0}^{\infty} \text{Cos}(mk_y y) \sum_{n=0}^{\infty} \left(a_{nm} \text{Cos}(nk_x x) + b_{nm} \text{Sin}(nk_x x) \right) \quad (2)$$

Both equations (1) and (2) utilise the fact that the experimental wave fields are symmetric in y (see section 3 below), although this is not a formal necessity. Furthermore, the series coefficients A_{nm} , B_{nm} , a_{nm} , b_{nm} are assumed to be functions of time only. In this form the velocity potential satisfies the governing field equation ($\nabla^2\phi=0$) representing mass continuity and the bottom boundary condition corresponding to a flat impermeable bed ($\phi_z=0$ on $z=-d$). The remaining constraints represent the nonlinear free surface boundary conditions (both kinematic and dynamic) evaluated on the water surface ($z=\eta$). After some re-arrangement these can be written as:

$$\Phi_t = -\left(g\eta + \frac{1}{2}(\Phi_x^2 + \Phi_y^2 + \Phi_z^2)\right) \quad (3)$$

$$\eta_t = \Phi_z - (\Phi_x\eta_x + \Phi_y\eta_y) \quad (4)$$

where g is the acceleration due to gravity.

Longuet-Higgins and Cokelet (1976) were the first to note that in this form the right hand side of equations (3) and (4) involve no time derivatives. As a result, if an initial spatial description of the water surface elevation, $\eta(x,y,z)$, and its associated velocity potential, $\phi(x,y,z)$, are known, it is possible to time-march the solution such that η and ϕ can be defined at all subsequent times. In the present cases the initial conditions, at some early time prior to the occurrence of a large wave event, can be calculated from linear or second-order theory on the basis that the wave group is fully dispersed. To apply this procedure it must be assumed that no significant wave energy lies above the truncation wave numbers Nk_x and Mk_y . Provided this is indeed the case, equations (3) and (4) can be solved at $2N(M+1)$ spatial locations in order to define the time derivatives of the coefficients $(A_{nm}, B_{nm}, a_{nm}, b_{nm})$. This corresponds to a grid spacing equal to half the wavelength of the shortest wave component. Once the time derivatives of the coefficients have been determined, the solution can be time-stepped using the Adams, Bashford, Moulton formulation (Gear, 1971) and the solution procedure repeated.

Within the present scheme the time derivatives of the free surface coefficients may be evaluated using a Fast Fourier Transform (FFT). Unfortunately, the time derivatives of the velocity potential are functions of η , and must be evaluated by solving a set of linear simultaneous equations using a lower-upper (LU) matrix decomposition. As a result, the numerical formulation is time consuming, and requires parallel computing power for the steepest directional wave cases. The present numerical formulation was implemented on a Fujitsu AP1000 parallel computer. On this machine the most computationally demanding wave groups may be evaluated accurately with run times of up to 16 hours. Full details of this numerical procedure are given in Johannessen and Swan (1998a).

3. Experimental Investigation

The purpose of the experimental study was to investigate a large number of focused wave groups in which the underlying wave components were spread in both the frequency and the directional domains. The experimental work was undertaken in the wide wave basin at the University of Edinburgh. This facility has a plan area of 25m x 11m, a uniform water depth of 1.2m, and is equipped with 75 numerically controlled wave paddles each 0.3m wide. To limit the occurrence of reflected waves, large passive absorbers were located at the downstream end of the wave basin and along one of the side-walls. A sketch showing the layout of this facility is given on figure 1.

Preliminary tests confirmed that within this facility waves could be generated within a directional range of $\theta = \pm 45^\circ$ and a frequency range of $0.6\text{Hz} \leq f \leq 1.7\text{Hz}$. Within the present tests, three separate frequency spectra were investigated. The first corresponds to a broad-banded spectrum (denoted by case B), and includes waves within the period range $0.6\text{s} \leq T \leq 1.4\text{s}$; while the second corresponds to a narrow-banded spectrum (denoted by case D), and includes waves within the period range $0.8\text{s} \leq T \leq 1.2\text{s}$. The third spectrum (denoted by case C) is intermediate to cases B and D and corresponds to a period range of $0.7\text{s} \leq T \leq 1.3\text{s}$. Within each of these cases a large number of wave

components, of equal amplitude, were uniformly spaced within the respective period range. This gives a corresponding amplitude spectrum, $a(f)$, which, in each case, decays according to f^{-2} (figure 2a).

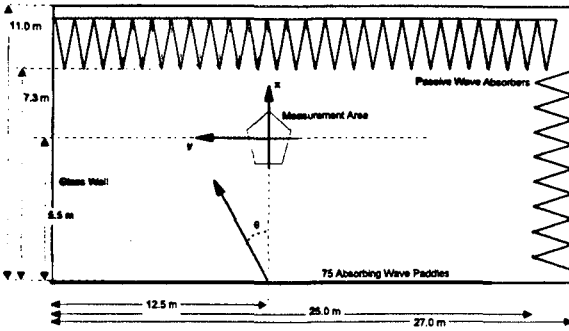


Figure 1: Experimental apparatus.

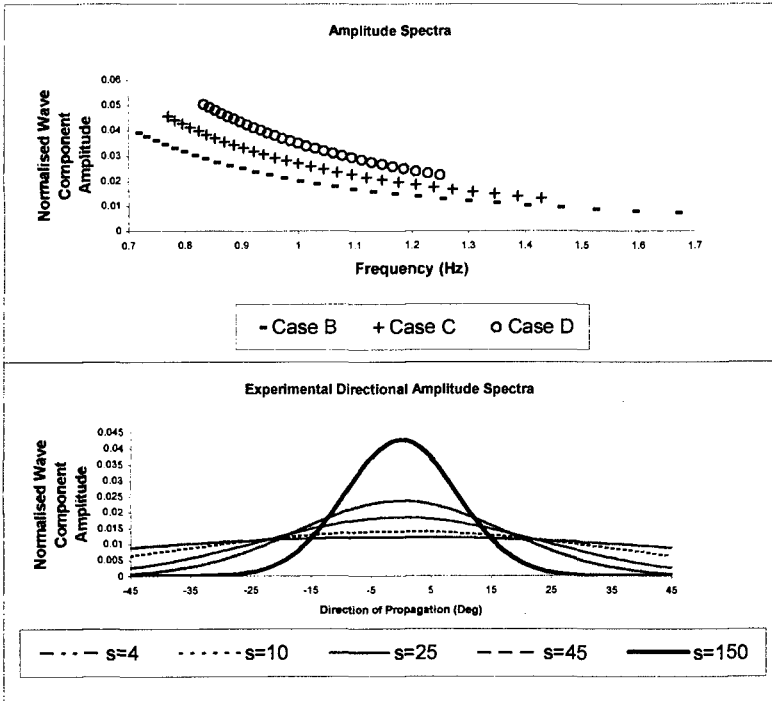


Figure 2a-b: Experimental amplitude spectra.
(a) In the frequency domain, (b) In the directional domain.

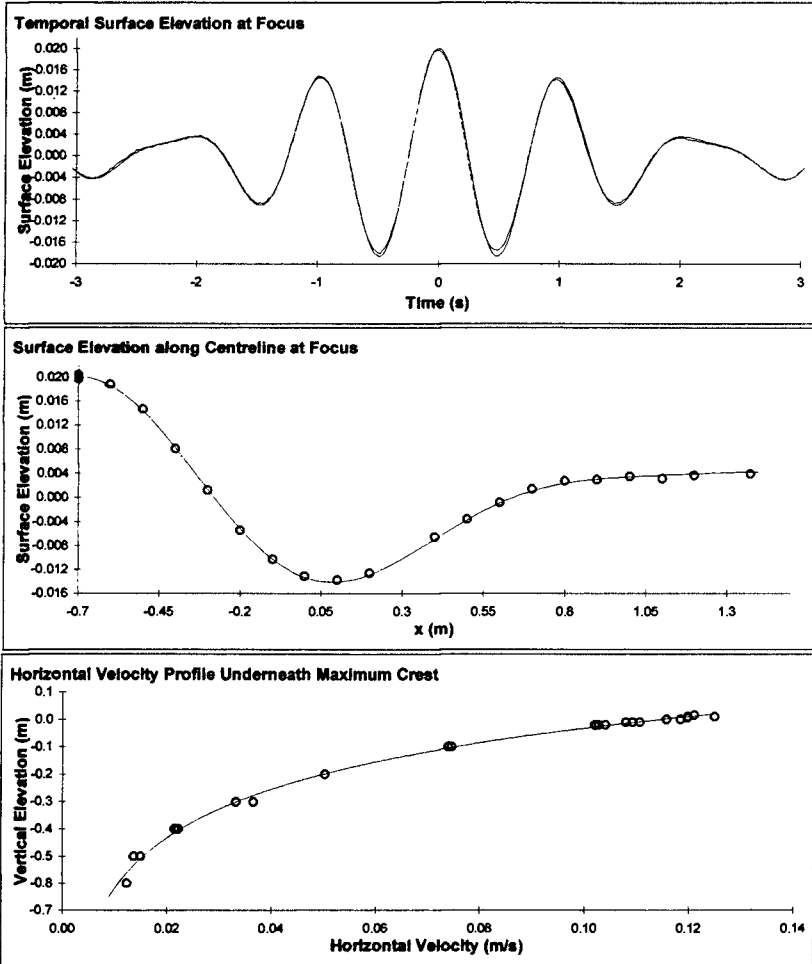
To quantify the directional spread of the wave components, the Mitsuyasu spreading parameter, s , was employed, where the directional amplitude spectrum, $a(\theta)$, is defined by:

$$a(\theta) = \lambda \cos^s(\theta/2) \quad (5)$$

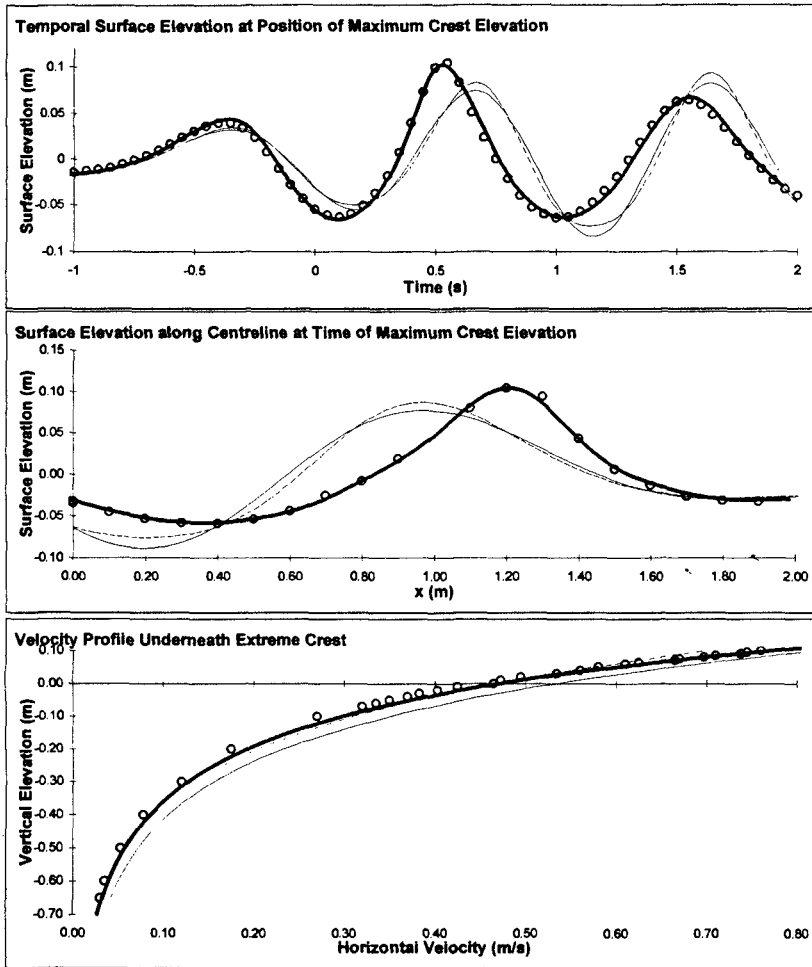
where θ denotes the wave direction measured relative to the x-axis and λ is a normalising coefficient. For each of the three frequency spectra, 6 directional spreads were adopted ($s=\infty, 150, 45, 25, 10, 4$); where $s=\infty$ corresponds to a unidirectional wave field, $s=150$ a very long-crested wave field, and $s=4$ a short-crested wave field. Graphical representations of these directional spreads are given on figure 2b. For each combination of frequency and directional spread a minimum of 4 input amplitude sums (A) were employed, where A corresponds to the linear sum of the component wave amplitudes. To address the widest range of wave conditions, the input amplitudes for each case were increased from $A=20\text{mm}$ (corresponding to a linear wave group) to $A=A_{\text{max}}$, where the latter values correspond to the onset of incipient wave breaking. In total some 88 individual wave groups were considered. A full discussion of this data is outside the scope of the present paper and is given in Johannessen and Swan 1998b.

For each of the wave fields described above, the surface elevation was sampled at 45 spatial locations in the vicinity of the linearly predicted focus position ($x=0, y=0$). These measurements were made using standard surface-piercing wave gauges that are estimated to have an accuracy of $\pm 1\text{mm}$. In addition, for a number of selected wave cases (15 in total) the x-component of the horizontal wave-induced velocity was recorded at closely spaced vertical elevations underneath the measured position of the maximum crest elevation. This velocity data was obtained using a one component laser Doppler anemometer that was estimated to have an accuracy of $\pm 2\%$.

As part of our preliminary measurements, considerable time was spent calibrating and validating the wave basin. The usual problems associated with wave reflections, which are notoriously strong in many wave basins, did not pose a significant problem in the present study. This is because the nature of a focused wave group is such that the waves are almost completely dispersed when they reach the downstream absorbers. Consequently, any energy reflected or scattered from the wave absorbers is negligible when compared with the energy density in the vicinity of the extreme event. The success of the calibration process is clearly demonstrated in figures 3a-3c. These results concern the narrow-banded wave spectrum (case D), with the largest possible directional spread ($s=4$, corresponding to a very short-crested sea state), and an input amplitude of $A=20\text{mm}$. This represents the smallest input amplitude and should, therefore, be in good agreement with a linear model. Figure 3a concerns the time-history of the water surface at the focus position, $\eta(t)$; figure 3b describes a spatial description of the surface elevation along the centreline $\eta(x)$; and figure 3c describes the horizontal velocity profile, $u(z)$, beneath the maximum crest elevation. In all cases the measured data is in very good agreement with the linearly predicted behaviour. Agreements of this type are essential if one is to interpret the nature of the nonlinear wave-wave interactions arising with larger input amplitudes.



Figures 3a-3c: Comparisons with a linear wave group.
 — linear theory; ———, o experimental data.



Figures 4a-4c: Comparisons with a nonlinear wave group.
 o experimental data; — numerical model; - - - linear theory;
 second-order theory .

4. Discussion of Results

Figures 4a-4c again concern the narrow-banded spectrum (case D) with a large directional spread ($s=4$), but now corresponds to a highly nonlinear wave group with an input amplitude of $A=93\text{mm}$. In this case the measured data is compared to the results of the numerical model (section 2), a linear solution, and a second-order solution based upon the wave-wave interactions identified by Longuet-Higgins and Stewart (1960) and further considered by Sharma and Dean (1981). In each of these figures the results of the numerical model are in very good agreement with the measured data. Furthermore, figure 4a, which concerns the time-history of the water-surface elevation measured at the position of the maximum crest elevation, suggests that the largest wave crest occurs after the linearly predicted focus event ($t=0$). Similarly, figure 4b, which presents a spatial description of the water surface elevation at the time of the maximum crest elevation, suggests that the largest wave crest also occurs downstream of the linearly predicted focus ($x=0$). These shifts in the focus time and position are consistent with those observed in unidirectional wave groups (Baldock et al., 1996). Furthermore, comparisons between the measured data and both the linear and the second-order solutions, suggest that significant energy shifts occur in the vicinity of the largest wave event.

In figure 4c comparisons with the horizontal velocity data, recorded beneath the largest wave crest, again confirm that the numerical model provides the best description of the measured data. However, the data also appears to be in reasonable agreement with the second-order solution, with the exception of a 15% under-prediction that arises very close to the water surface. This latter result is in marked contrast to the unidirectional data presented by Baldock et al. (1996).

To further examine the success of the numerical model, figure 5 again concerns frequency spectrum D, with $s=4$ and $A=93\text{mm}$. In this figure, time-histories of the water surface elevation are presented at four spatial locations: $x=0$, or the linearly predicted focus position; $x=0.6\text{m}$; $x=1.2\text{m}$, which is the observed position of the maximum crest elevation; and $x=1.8\text{m}$. At each of these locations the numerical model is in good agreement with the measured data, and is shown to be very different from either the linear or the second-order solutions.

To isolate the effect of the directional spread, two further comparisons were undertaken. Firstly, the linear sum of the component wave amplitudes generated at the wave paddles were held constant ($A=55\text{mm}$), and the global maximum crest elevations measured for a range of directional spreads for each frequency spectrum. This data is presented on figure 6a. Comparisons between these results clearly suggest that the effect of introducing a directional spread is to dramatically reduce the maximum crest elevation. Furthermore, the bulk of this reduction occurs between a unidirectional wave group ($1/s=0$, where s is again the Mitsuyasu spreading parameter) and a long-crested wave group with small directional spread. Since the local increase in the crest elevation (above that predicted by linear theory) arises due to the nonlinear wave-wave interactions, and almost certainly involves a shift of energy into the higher frequencies, the data presented

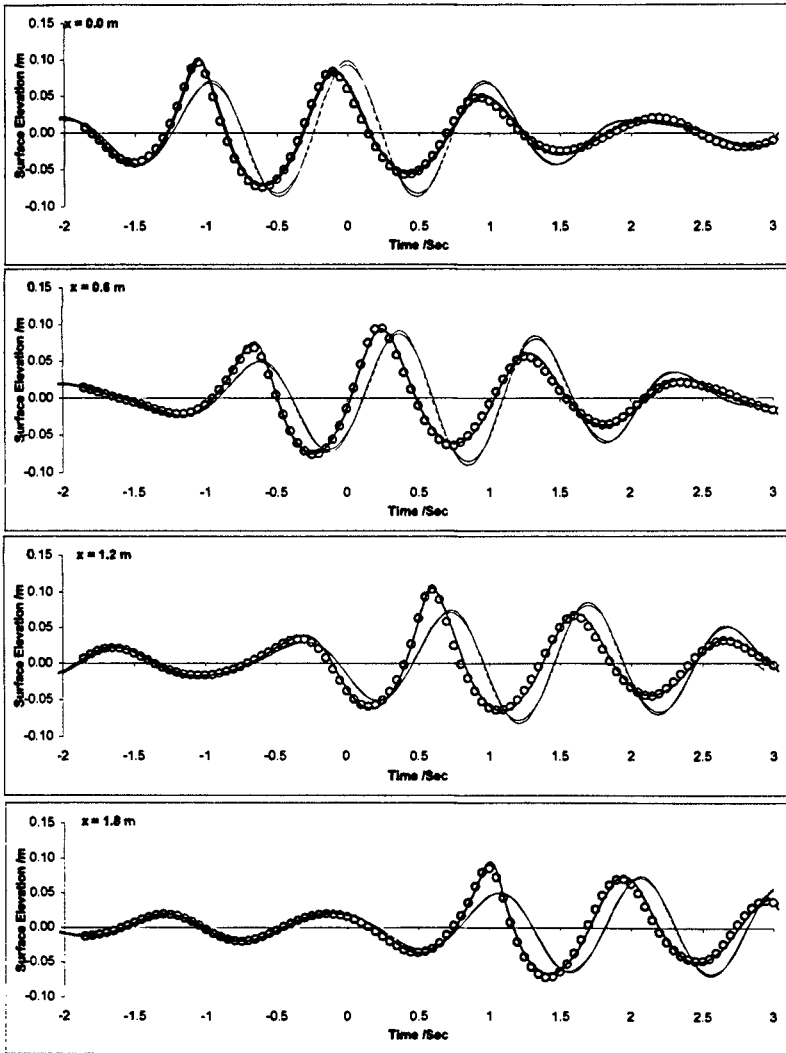
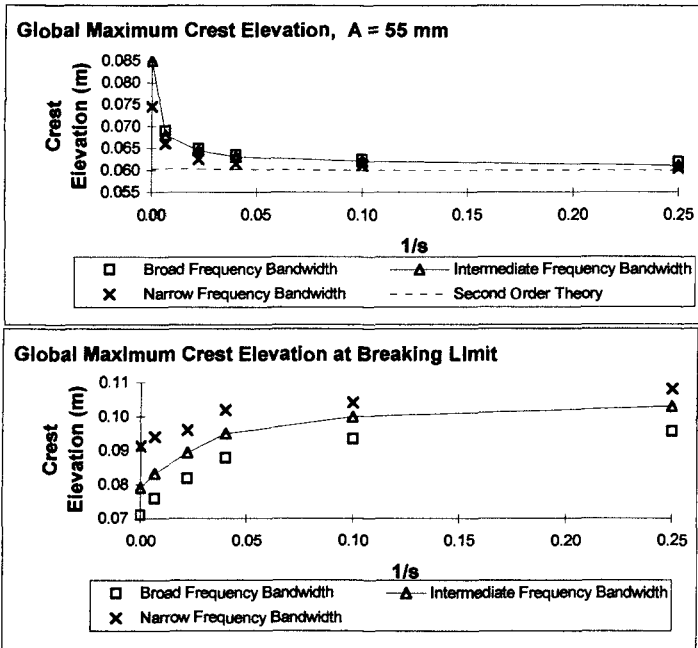


Figure 5: Evolution of a nonlinear wave group.

— experimental data; ○ numerical model; — linear theory;
 - - - second-order theory .

on figure 6a represents a weakening of the nonlinear wave-wave interactions due to the underlying directionality. Although further analysis of this data is required, it is believed that this effect is caused by a reduction in the absolute wave front steepness and curvature. This is due to the fact that in a directional wave this steepness can be distributed around the perimeter of the wave, and is not constrained in one plane. If this is indeed the case, it clearly explains why extreme unidirectional waves (generated in the laboratory) appear more nonlinear than those observed in the open ocean.

The data presented on figure 6a also has implications for the limiting wave height. If increasing directionality reduces the nonlinearity, this perhaps implies that a larger linear amplitude sum (A) is required to induce incipient wave breaking. To examine this point, a second set of comparisons were undertaken in which the amplitude of the wave components generated at the wave paddles was progressively increased until there was evidence of incipient wave breaking in the vicinity of the focus position. This allowed the variation in the maximum possible crest elevation, for a given underlying frequency bandwidth, to be recorded as a function of the directional spread. This data is presented on figure 6b and clearly suggests that the limiting crest elevation increases with the directional spread. Indeed, figure 6b suggests that the difference between a unidirectional wave group ($1/s=0$) and a short-crested wave group (with $1/s=0.25$) can lead to an increase in the limiting crest elevation by as much as 25%.



Figures 6a-6b: Maximum crest elevation. (a) $A=55\text{mm}$, (b) $A=A_{\text{max}}$.

5. Nonlinear Interactions and Energy Shifts

To examine the nature of the nonlinear wave-wave interactions and the associated energy shifts, the numerical model was used to simulate the narrow-banded spectrum (case D) with four different directional spreads. In each of these cases the input amplitude sum (A) was such that the largest waves were on the limit of wave breaking. Details of the directional spreads and the input amplitudes are given in table 1.

Wave case.	Directional spread, s .	Input amplitude, A
1	∞ (Unidirectional)	61mm
2	150	71mm
3	45	78mm
4	4	93mm

Table 1: Numerical simulations

Applying a Fast Fourier Transform to the numerically predicted time-history of the water surface elevation, $\eta(t)$ at the position of the largest wave crest allowed the frequency content to be accurately defined. The results of this analysis, applied to each of the wave cases given on table 1, are present on figure 7. In addition, the solid line indicated above the power spectra defines the linear input of the wave components generated at the paddles (for $s=4$, $A=93\text{mm}$), while the dashed lines indicated on the right hand side of the figure define the range of the second-order frequency sum terms.

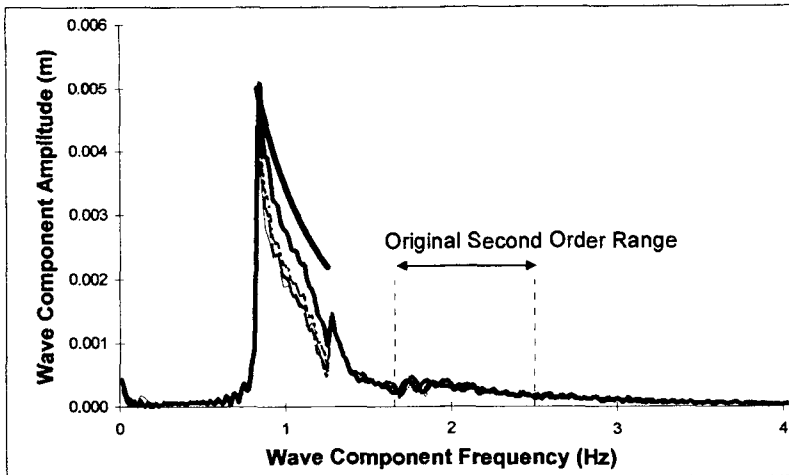


Figure 7: Frequency spectra.

These results clearly suggest that there is a 'loss' of energy from within the linear input range. However, this energy is not primarily transferred to the second-order frequency-sum terms, as one might expect, but appears as significant energy at frequencies just larger than the upper limit of the linear input range (ie. $\approx 1.3\text{Hz}$). Furthermore, although the energy distribution within the linear input range varies between the four cases, due to the different linear amplitude sums; the energy immediately outside the linear range appears to be virtually identical. Given that each of these waves is on the limit of incipient wave breaking, it would seem plausible that the growth of energy within these high frequencies plays a major role in defining the characteristics of extreme wave groups. Furthermore, the energy level indicated on figure 7 appears to represent a threshold value beyond which wave breaking will occur. Detailed analysis of these observed energy transfers is provided by Johannessen and Swan (1998b).

6. Concluding Remarks

The nonlinear evolution of a large number of directional wave groups has been investigated experimentally, and a new numerical model shown to be in good agreement with the laboratory data. The principle advantage of this numerical model is that it represents the only solution that rigorously includes nonlinearity, unsteadiness and directionality. Furthermore, it does not require a detailed description of the nonlinear water surface profile (something which is seldom available in practice) since it is based upon a linear description of the underlying wave spectrum. From a practical point of view the results presented in this paper confirm that for a given linear crest height (or input amplitude sum, A) and frequency bandwidth, the effect of increasing directionality is to significantly reduce the nonlinearity of a wave group. This explains the significant differences between two-dimensional wave flume experiments and field data. However, as a consequence of this reduced nonlinearity, the maximum nonlinear crest elevation that may be obtained, before further growth is limited by wave breaking, increases with the directionality of the wave field provided the frequency bandwidth is held constant. This has important implications for the specification of a 'design' wave, and highlights the need to fully include the nonlinearity, unsteadiness and directionality in both model testing and numerical calculations.

Acknowledgements

The present study has formed part of the research programme 'Uncertainties in Loads on Offshore Structures' sponsored by EPSRC through MTD Ltd and jointly funded with: Amoco (UK) Exploration Company, BP Exploration Operating Co Ltd, Brown & Root Ltd, Exxon Production Research Company, Health and Safety Executive, Norwegian Contractors a.s., Shell UK Exploration and Production, Den norske Stats Oljeselskap a.s. and Texaco Britain Ltd. EPSRC Grant Reference GR/J23976. The authors are also grateful for further funding from the Norwegian Research Council (norges Forskningsråd).

References

- Baldock, T.E. & Swan, C. (1994), 'Numerical calculations of large transient water waves', *Appl. Ocean Res.*, **16**, pp 101-112.
- Baldock, T.E., Swan, C. & Taylor, P.H., (1996), 'A laboratory study of non-linear surface waves on water', *Phil. Trans. Roy. Soc. London, Ser. A*, **354**, pp 649-676.
- Dean, R.G., (1965), 'Stream function representation of non-linear ocean waves', *J. Geophys. Res.*, **70**, pp 4561-4572.
- Dold, J.W. & Peregrine, D.H., (1984), 'Steep unsteady waves: an efficient computational scheme', *Proc. 19th Int. Conf. Coastal Engineering, ASCE*, **1**, pp 955-67.
- Dommermuth, D.G., Yue, K.P., Lin, W.M. & Rapp, R.J. (1988). 'Deep-water plunging breakers: a comparison between potential theory and experiment.' *J. Fluid Mech.*, **189**, pp 423-442.
- Fenton, J.D. (1985), 'A fifth order Stokes' theory for steady waves', *J. Waterways, Port, Coastal and Ocean Engng.*, **111**, pp 216-234.
- Fenton, J.D. & Rienecker, M.M., (1980), 'Accurate numerical solutions for nonlinear waves', *7th Int. Conf. on Coastal Engng., Sydney*, **1**, pp 50-69.
- Gear, S.W., (1971), 'Numerical initial value problems in ordinary differential equations', Englewood Cliffs Inc., Prentice Hall.
- Johannessen, T.B. & Swan, C. (1998a), 'A Fourier solution for three-dimensional surface water waves. Submitted to *J. Fluid Mech.*
- Johannessen, T.B. & Swan, C. (1998b), 'A laboratory study of directionally spread surface waves on water'. Submitted to *Phil. Trans. Roy. Soc. Ser. A*.
- Jonathan, P., Taylor, P.H. & Tromans, P.S., (1994), 'Storm Waves in the Northern North Sea', *Proc. 7th Int. Conf. on the Behaviour of Offsh. Str., Mass.*, **2**, pp 481-494.
- Longuet-Higgins, M.S. & Stewart, R.W., (1960) 'Changes in the form of short gravity waves on long waves and tidal currents', *J. Fluid Mech.*, **8**, pp 565-583.
- Longuet-Higgins, M.S. & Cokelet, E.D., (1976), 'The deformation of steep surface waves on water. A numerical method of computation', *Proc. Roy. Soc., Ser. A*, **350**, pp 1-26.
- Rozario, J.B., Tromans, P.S., Taylor, P.H. & Efthymiou, M., (1993), 'Comparisons of loads predicted using 'New Wave' and other wave models with measurements on the Tern structure', In: 'Wave Kinematics and Environmental Forces', *Soc. Underwater Tech., Kluwer*, **29**, pp 143-158.
- Sharma, J.N. & Dean, R.G., (1981), 'Second-Order Directional Seas and Associated Wave Forces', *Society of Petroleum Engineers J.*, **4**, pp 129-140.
- Smith, S., & Swan, C., (1996), 'Kinematic predictions in large shallow water waves', *Proc. 25th Int. Conf. Coastal Engng., Orlando, Florida*, **1**, pp 502-515.
- Tromans, P.S., Anaturk, A. & Hagemeijer, P., (1991), 'A new model for the kinematics of large ocean waves - application as a design wave', *Proc. 1st Int. Offshore and Polar Engng. Conf.*, **3**, Edinburgh, pp 64-71.